Surface transparency in ^{12}C elastic scattering from $^{40,42,48}Ca$

T. R. Renner
Department of Physics, University of Chicago, Chicago, Illinois 60637
and Argonne National Laboratory, Argonne, Illinois 60439
(Received 20 July 1978)

Angular distributions between 3 and 110 degrees in the laboratory system were measured for the elastic scattering of ^{12}C from $^{40,42,48}Ca$ at 51.0, 49.9, and 47.2 MeV, respectively. Pronounced oscillations were observed in the $^{12}C + ^{40}Ca$ angular distribution. Weaker oscillations were observed in the $^{12}C + ^{42}Ca$ angular distributions while none were seen in $^{12}C + ^{48}Ca$. An optical-model analysis was performed using Woods-Saxon and folded potentials. Surface transparent potentials were found to parametrize the oscillatory structure of the forward-angle data of $^{12}C + ^{40}Ca$. Stronger surface absorption in the $^{12}C + ^{42,48}Ca$ imaginary potentials apparently weakens or washes out any forward-angle oscillations. Optical potentials that fit forward-angle data of $^{12}C + ^{40}Ca$ also predict oscillatory structure in the excitation function at 180°.

[NUCLEAR REACTIONS $^{40}Ca(^{12}C, ^{12}C)^{40}Ca$, $E = 51$ MeV; measured $\sigma(\theta)$, measured $\sigma(E, \theta = 180°)$. $^{42}Ca(^{12}C, ^{12}C)^{42}Ca$, $E = 49.9$ MeV; $^{48}Ca(^{12}C, ^{12}C)^{48}Ca$, $E = 47.2$ MeV; measured $\sigma(\theta)$.]

I. INTRODUCTION

A. α elastic scattering

The anomalous large-angle elastic scattering (often called ALAS) of α particles from ^{40}Ca has long been an interesting phenomenon without a completely satisfactory solution.[1] The unusual "enhancement" of the elastic cross section around 180° is observed at α energies from about 18 MeV up to at least 30 MeV. The observed cross section is larger than the Rutherford cross section and is approximately two orders of magnitude greater than found in heavier nuclei. Many parametrizations of the experimental data have been proposed and are referred to in the literature by the following terms: (i) α exchange,[2] (ii) surface-transparent potentials,[3] (iii) Regge poles,[4] (iv) L-dependent absorption,[5] (v) modified Woods-Saxon potentials.[6] All of these approaches can fit the angular distributions, at least at one energy, by modifying the phase shifts of the grazing partial waves from the values they would have with more strongly absorbing potentials.

However, an important feature of the data is not explained: the dependence of the back-angle enhancement on the atomic weight of the target.[7] For example, a single neutron added to the $1f_{7/2}$ shell, as in ^{41}Ca, does not significantly alter the effect while the enhancement disappears when two or more neutrons are added to ^{40}Ca as in $^{42,44,48}Ca$. Furthermore, data from the elastic scattering of α's from other nuclei near ^{40}Ca show similar characteristics: ^{38}Ar, ^{39}K, and ^{40}K have enhanced back-angle elastic cross sections but ^{40}Ar and ^{41}K, each of which has two $1f_{7/2}$ neutrons, do not.

A comparable dependence on atomic weight has also been observed in the measurements of fusion cross sections with heavy-ion projectiles on targets of p and sd-shell nuclei.[8,9] The work, performed at Argonne, shows a pronounced difference in the maximum fusion cross section for nuclei in the same shell compared with nuclei in different shells. For example, the $^{12}C + ^{18}O$ fusion cross section saturates at a value ~1.2 times larger than does $^{12}C + ^{16}O$. This difference has been attributed to a difference in the fusion radii of these two nuclei, which may be a consequence of the larger valence orbits of the two $1d_{5/2}$ nucleons in ^{18}O. The extra nucleons may increase the absorptive radius over that of ^{16}O by increasing the number of reaction channels leading to fusion.

Back-angle enhancements have also been seen in the elastic scattering of protons from nuclei near ^{40}Ca.[10] ^{3}He elastic scattering from the calcium isotopes[11] also shows a similar, but smaller, effect with the same A dependence as found in ALAS, i.e., the enhancement is present in ^{3}He scattered from ^{40}Ca and absent for ^{3}He scattered from $^{44,48}Ca$.

The occurrence of anomalous large-angle scattering and its dependence on valence neutrons in heavy-ion scattering will be discussed further, but first we will review the various parametrizations listed above, for the large-angle anomalous scattering of α's from ^{40}Ca.

i. α exchange. The exchange of the incident particle with an α cluster in the target nucleus is assumed to cause the enhancement at back angles. Only clusters on the surface of the target nucleus should contribute; hence, surface partial

waves ($L=KR$ where R is the nuclear radius) will contribute the most to the effect.[2]

ii. Surface transparent potentials. An optical-model fit to the data is achieved using an imaginary potential which is surface transparent, i.e., grazing or surface partial waves are weakly absorbed. Their contribution to the scattering amplitude again dominates that of other partial waves at back angles.[3]

iii. Regge-pole analysis. A Regge-pole parametrization of the data defines the S matrix as a function of L to be a background term times a Breit-Wigner resonance form in angular momentum space. The effect of the Regge pole is to accentuate the importance of a particular L value and in this case it is chosen to be the surface partial wave.[4]

iv. L-dependent absorption. An optical potential having an imaginary well with an angular momentum cutoff is used to calculate the elastic scattering. The idea here is that high partial waves that bring in more angular momentum than can be carried away in reactions or inelastic scattering remain in the elastic channel; the result is to enhance the contribution of the grazing partial waves.[5]

v. Modified Woods-Saxon potentials. Fits to the elastic α scattering have been achieved by using a Woods-Saxon form factor raised to an adjustable power in the complex optical potential. The adjustable power of the Woods-Saxon geometry allows greater freedom of the surface shape of the potential where elastic scattering occurs.

B. Heavy-ion studies

Recent results of ^{16}O elastic scattering from ^{28}Si display features similar to the anomalous α scattering.[12] An enhancement in the observed cross section was found at back angles; similar results have been obtained for ^{12}C on ^{28}Si.[13] While the ratio of the cross section to the Rutherford cross section is typically only 10^{-2} in both cases, it is still approximately two orders of magnitude larger than the ratio around 90°. The angular distributions at back angles have a periodicity of a pure Legendre polynomial squared, with an L value close to the surface partial wave. A Regge-pole parametrization of the angular distributions has been made as well as an optical-model fit using surface transparent potentials.

In addition, an excitation function at 180° shows pronounced resonancelike structure in both systems. This structure is indicative of processes with time scales on the order of transit times across the nucleus. The simplest such processes are the shape resonances produced from the interference of incoming partial waves inside the scattering potential.

C. Justifications for the present work

The large overlap of the ^{12}C ground state with three α particles suggested that behavior similar to that seen in the α-particle elastic scattering might be observed in the ^{12}C elastic scattering from ^{40}Ca. Measurement of the elastic scattering from ^{42,48}Ca enabled us then to study the effect of the additional $1f_{7/2}$ valence neutrons on the elastic scattering. An excitation function taken at 180° measured the energy behavior of the back-angle cross section; reasonancelike structure and enhancement of the cross section, as seen in the ^{12}C, ^{16}O + ^{28}Si elastic scattering at 180°, was looked for.

Whether behavior for the ^{12}C scattering similar to the α scattering from ^{40}Ca might occur for similar energies, similar momenta, or similar momentum transfers was not known. Nor was it known if perhaps the momentum and energy of the individual constituent α particles with the ^{12}C nucleus were relevant parameters. For α particles, the onset of the ALAS effect around 16.4 MeV (c.m.) corresponds to an energy of ~7 MeV above the Coulomb barrier. The equivalent energy above the 24-MeV Coulomb barrier of ^{12}C on ^{40}Ca would be 31 MeV in the c.m. frame. This was felt to be a minimum energy; a higher bombarding energy for the ^{12}C was chosen so that a probe of the nuclear potential at higher momentum transfers could be made. A ^{12}C lab energy readily and consistently obtained with the Argonne tandem accelerator was 51 MeV. This energy allowed for total momentum transfers up to ~2.5 times that in the α-particle scattering. At this energy only for very small momentum transfers is the process dominated by the Coulomb field. The quarter-point angle[14] where $\sigma/\sigma_R = 0.25$ was 39° (c.m.); this marks the beginning of strong nuclear absorption removing flux from the elastic channel.

II. EXPERIMENTAL PROCEDURE

The angular distributions were measured using the Argonne FN tandem accelerator and the 70-in. scattering chamber. Data were recorded and analyzed on a PDP11/45 computer with the data-acquisition program SNAP. The 51-MeV laboratory energy of the ^{12}C ion corresponded to a center-of-mass energy of 39.2 MeV. Assuming a constant center-of-mass momentum for the three systems, ^{12}C + ^{42,48}Ca center-of-mass energies were 38.8 and 37.7 MeV, respectively. At these energies of approximately 15 MeV above the Coulomb barrier, a Fresnel diffraction[15] pattern char-

acterizes the angular distributions. The maximum classically allowed scattering angle, or "rainbow angle,"[16] is around 25°. Classically the deflection function, which describes scattering into an angle θ as a function of angular momentum L or impact parameter b (since $L=kb$), is a maximum at the rainbow angle. Scattering for angles forward of the Coulomb rainbow is essentially Rutherford scattering ($\sigma/\sigma_R \sim 1$) since here impact parameters are so large that only the Coulomb force is felt. Past the rainbow angle one begins to probe the nuclear force and the ratio of σ/σ_R falls off exponentially as flux is removed from the elastic channel by nuclear absorption.

Our work consisted then of three separate experiments. Each measurement involved a different angular region with its own set of considerations and difficulties. The three regions were (a) very forward-angle data where $\theta \leq 20°$, (b) middle-angle data where $20° \leq \theta \leq 65°$, and (c) large-angle data where $65° \leq \theta \leq 110°$. The targets in all the experiments varied from 50 to 200 $\mu g/cm^2$ and were made from enriched calcium isotopes evaporated on a 10 $\mu g/cm^2$ carbon backing. An energy loss of at most only a few hundred keV by the ^{12}C in the targets allowed the resolution of the ground state from the excited states of the calcium isotopes and from the Doppler broadened 4.33-MeV state of ^{12}C.

A. Forward-angle data: $\theta_{c.m.} \leq 20°$

The elastic scattering in this region is Coulomb dominated implying large cross sections. A small solid-angle aperture, typically 2×10^{-6} sr, was used with a single silicon detector to reduce the count rate to a reasonable level. At very forward angles $\theta < 8°$ the $\sin^{-4}(\theta/2)$ dependence of the Rutherford cross section changes rapidly with angle; uncertainties of 0.05° at 3° make 7% changes in the cross section. To achieve absolute normalizations of the order of 5% then, precise angle measurements were necessary. Fixed left and right monitor detectors were used to determine angle corrections arising from asymmetries of the beam with respect to the center line of the scattering chamber. Assuming the cross sections are purely Rutherford for $\theta < 6°$ and knowing angles to an accuracy of 0.05° allowed us to normalize our data. Absolute cross section errors are believed to be between 5 and 10%.

Identification of the elastic peak was unambiguous at these angles, but ubiquitous ^{12}C and ^{16}O contaminants in the targets contributed to the scattering yield at very forward angles. A measurement of the ^{12}C and ^{16}O content in the target was made when the ^{12}C + Ca elastic peak and ^{12}C + ^{12}C, ^{12}C + ^{16}O peaks were distinguishable; a correction to the elastic yield was then made when they overlapped.

B. Middle angles: $20° \leq \theta_{c.m.} \leq 65°$

The middle-angle data were obtained with three silicon surface-barrier detectors placed 15° apart on a rigid base. All three had apertures with approximately equal solid angles of 2.2×10^{-3} sr. Three simultaneous measurements were made in this way. By repeating data points at a given angle with each detector, relative normalizations between detectors were obtained. Peak identification and background were not problems in these measurements.

C. Large angles: $65 \leq \theta_{c.m.} \leq 110°$

Cross sections in this region were between 5 and 50 μb making single-angle measurements very time consuming. For this reason a position-sensitive Si surface barrier detector with an active surface area of 8×47 mm was placed 5 cm from the target to take the remaining large-angle data. The outputs of the detector gave energy and position information of the detected particles. The angle calibration of the detector was made by placing three wires, whose positions were known, in front of the detector. An energy calibration of the spectrum utilized 51-MeV ^{12}C ions elastically scattered from ^{197}Au and 30-MeV ^{12}C ions elastically scattered from ^{58}Ni and ^{197}Au.

The observed spectrum contained the elastic peak and a background corresponding to energies $\lesssim$15 MeV. As the energy of the elastic ^{12}C particles fell below 15 MeV for $\theta > 110°$, the elastic peak became inseparable from the background. An attempt to eliminate this background was made by using self-supporting ^{40}Ca foils in hopes of eliminating any reaction products from the ^{12}C projectile with the ^{12}C backing used in the original targets; unfortunately no noticeable change in the background resulted. Presumably the background came from ^{12}C + ^{40}Ca reaction products; consequently, measurements beyond 110° could not be made. A subsequent measurement of the excitation function at 180° was made by reversing the reaction, i.e., ^{12}C(^{40}Ca, ^{12}C)^{40}Ca. The much larger center-of-mass momentum here resulted in a much larger ^{12}C laboratory energy. These measurements are reported elsewhere.[20]

D. Results

The angular distributions of the scattering from the three isotopes (see Fig. 1) are very similar in general shape with a small shift in the rainbow

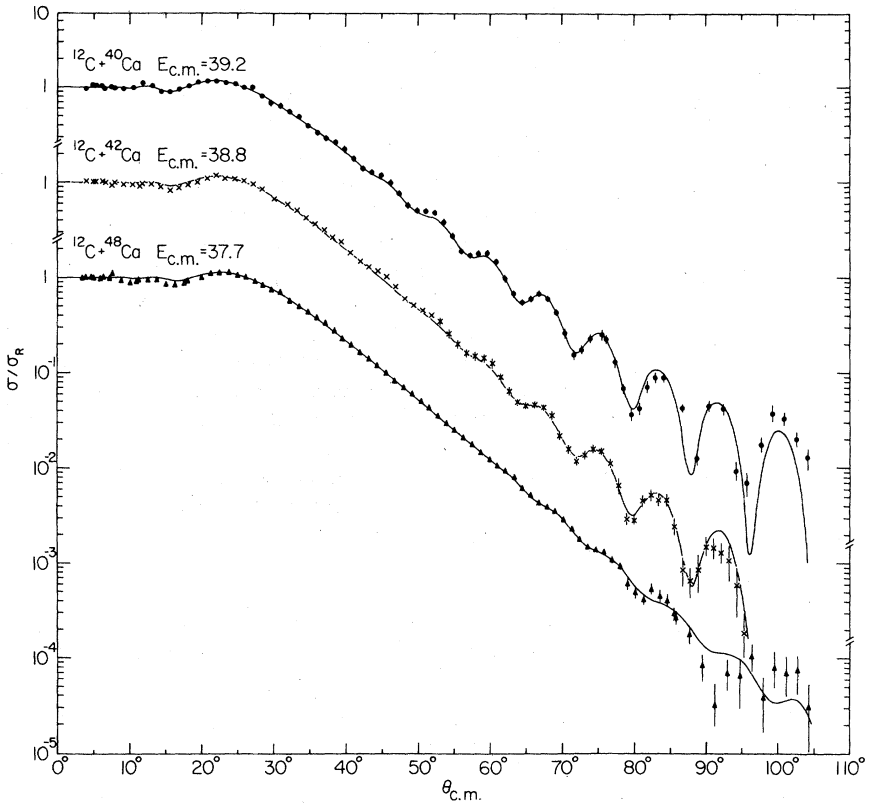

FIG. 1. (a) $^{12}C+^{40}Ca$ angular distribution at 51 MeV (lab) with optical-model fit using parameters found in Table II. (b) $^{12}C+^{42}Ca$ angular distribution at 49.9 MeV (lab) with optical-model fit using parameters in Table II. (c) $^{12}C+^{48}Ca$ angular distribution at 47.12 MeV (lab) with optical-model fit using parameters in Table II.

angle from one isotope to another. The exponential falloff of the cross sections for angles greater than the rainbow angle, as is usual in heavy-ion scattering, is seen in the ^{48}Ca data. However, a very pronounced oscillation superimposed on this shape is observed in ^{40}Ca. In ^{42}Ca damped oscillations, somewhat between the previous two cases, are seen. These differences are emphasized in Fig. 2 by plotting the data divided by the empirical factor $\exp(-0.15\times\theta)$. The implication of these differences will be analyzed and discussed in the next section.

III. DATA ANALYSIS

A. Optical-model analysis

1. Forward-angle data

Conventional analysis of elastic-scattering data with an optical model uses Woods-Saxon geometries for the real and imaginary potentials, i.e.,

$$U(r) = V(r) + i\,W(r) + V_c(r),$$

where

$$V(r) = V_o\{1+\exp[(r-R_R)/a_R]\}^{-1},$$

$$W(r) = W_o\{1+\exp[(r-R_I)/a_I]\}^{-1}$$

and V_c is the potential of a uniform charge distribution. This approach allows a maximum of six degrees of freedom when fitting elastic-scattering data. Often a unique determination of all the parameters is not possible though all six degrees of freedom are necessary to adequately reproduce the behavior of the data. In this analysis all six parameters $V_o, R_R, a_R, W_o, R_I, a_I$ were varied.

Fits to the data were obtained (Fig. 1) assuming an initial starting set of parameters for the real and imaginary Woods-Saxon potentials and searching to find a minimum in χ^2. The optical-model code PTOLEMY[17] was used with a Coulomb well calculated by folding two spherical charge distributions with experimentally determined rms charge radii. For ^{12}C on ^{40}Ca four families of parameters were found to give equally good fits; these four sets, found in Table I, agree well with those found by Morgan and Fletcher.[18]

In fitting the $^{12}C+^{42,48}Ca$ data the ^{40}Ca parameters of set 3 (Table I) were used as initial values for the Woods-Saxon parameters because they gave the smallest value of χ^2. The new sets of parameters shown in Table II were found in minimizing χ^2; the unmodified ^{40}Ca parameters were unable to adequately fit the data of the other isotopes. A study of the χ^2 space of $^{42,48}Ca$ was then made by varying various subsets of the six parameters $V_o, R_R, a_R,$

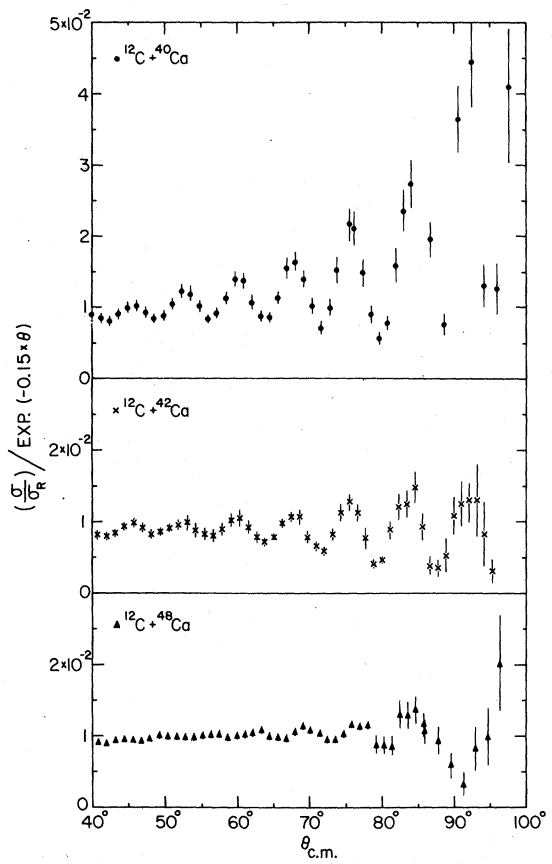

FIG. 2. Large-angle comparison of ^{12}C + ^{40,42,48}Ca data. Angular distributions were divided by exp(−0.15 × θ) before plotting.

W_o, R_I, a_I. As seen in Table III and IV most of the fit for ^{42,48}Ca could be achieved by varying one single parameter, the imaginary diffuseness a_I. The conclusion is clear: The imaginary potentials for ^{48}Ca and for ^{42}Ca have a more extended range than the imaginary potential of ^{40}Ca. The extra nucleons in the large $1f_{7/2}$ shell in these nuclei seem to extend the imaginary well possibly because there are many additional reaction channels available through them.

On the other hand ^{40}Ca seems to require a more surface-transparent potential as demonstrated in Fig. 3 by the transmission coefficients of the three systems. Clearly there is a much sharper cutoff in L space for ^{40}Ca than ^{42,48}Ca; fewer surface partial waves contribute to the nuclear scattering. This observation is true for all the ^{40}Ca parameter sets since all of them require more diffuse imaginary potentials when fitting ^{42,48}Ca.

As in the ^{16}O + ^{40}Ca elastic-scattering analysis[19] we find a unique radius of 8.6 fm at which all four real potentials of ^{12}C + ^{40}Ca agree. In Table V the critical angular momenta of the three systems are determined using two separate methods and are found to agree well with one another. The strong absorption radii are also given.

2. *Back-angle data*

The ^{40}Ca parameters for the forward-angle data were used to calculate an excitation function at 180° to compare with the data obtained from Ref. 20. The quantity

$$\sigma(E) = \int_{174°}^{180°} \frac{d\sigma}{d\Omega}(E) \sin\theta \, d\theta \Big/ \int_{174°}^{180°} \sin\theta \, d\theta$$

was calculated at energies between 28 and 35 MeV in 0.5-MeV steps and is plotted with the data in Fig. 4. Using these surface-transparent potentials the optical model predicts an oscillatory behavior of the right period and roughly the right magnitude, but shifted in phase. Certainly a fit to the data at forward angles at one energy cannot be expected to exactly fit the excitation function data taken at 180°. The fact that such oscillations do seem to occur in the calculations with surface-transparent potentials lends credibility to such a description of the scattering.

TABLE I. ^{12}C + ^{40}Ca Woods-Saxon optical-model parameters.

	V_0 (MeV)	R_R (fm)	a_R (fm)	W_0 (MeV)	R_I (fm)	a_I (fm)	χ^2/DF[c]
1	85.8[a]	6.74	0.45	11.1	6.9	0.5	
	76.8 ± 2.4	6.83 ± 0.08	0.512 ± 0.020	11.2 ± 2.2	6.7 ± 0.5	0.71 ± 0.12	1.7
2	153.8[a]	6.57	0.5	14.0	6.3	0.68	
	152.0 ± 2.7[b]	6.53 ± 0.06	0.501 ± 0.014	20.8 ± 6.9	5.6 ± 1.1	0.76 ± 0.19	1.9
3	49.4[a]	7.14	0.5	8.8	6.9	0.64	
	60.5 ± 2.4[b]	6.91 ± 0.09	0.518 ± 0.025	8.9 ± 1.6	7.1 ± 1.6	0.71 ± 0.11	1.6
4	495.6[a]	5.99	0.5	26.3	5.8	0.64	
	502.0 ± 10[b]	5.93 ± 0.08	0.498 ± 0.015	47.1 ± 28.4	4.5 ± 2.4	0.78 ± 0.33	2.1

[a] Florida State values.
[b] PTOLEMY best fit values. Uncertainties are rms uncertainties.
[c] χ^2/DF ≡ χ^2 per degree of freedom.

TABLE II. Optical-model parameters for $^{12}C + ^{40,42,48}Ca$.[a]

System	V_0 (MeV)	R_R (fm)	a_R (fm)	W_0 (MeV)	R_I (fm)	a_I (fm)	χ^2/DF[b]
$^{12}C + ^{40}Ca$	60.5 ± 2.4	6.91 ± 0.09	0.518 ± 0.025	8.87 ± 1.56	7.09 ± 0.42	0.707 ± 0.105	1.6
$^{12}C + ^{42}Ca$	70.2 ± 3.1	6.54 ± 0.13	0.590 ± 0.034	8.35 ± 1.03	7.32 ± 0.32	0.758 ± 0.083	1.5
$^{12}C + ^{48}Ca$	58.8 ± 2.2	6.74 ± 0.08	0.574 ± 0.018	10.0 ± 1.33	7.22 ± 0.28	0.817 ± 0.053	5.2

[a] Errors are rms errors.
[b] $\chi^2/DF \equiv \chi^2$ per degree of freedom.

TABLE III. ^{42}Ca parameter variation.[a]

V_0 (MeV)	R_R (fm)	a_R (fm)	W_0 (MeV)	R_I (fm)	a_I (fm)	χ^2/χ_0^2[b]
60.5	6.91	0.518	8.87	7.09	0.707	12.4
70.2	6.54	0.590	8.35	7.32	0.758	1.0
					0.922	1.9
		0.554				2.8
	6.94					10.7
			9.19			11.3
60.7						11.5
				7.10		11.5

[a] The first line is the set of parameters that fit the ^{40}Ca data (line 1) of Table II. The subsequent lines are least-squares fits to the data when various parameters were allowed to vary from the values given in the first line. No entry signifies that the values were held fixed at those given in the first line.
[b] $\chi_0^2 = 1.5$.

TABLE IV. ^{48}Ca parameter variation.[a]

V_0 (MeV)	R_R (fm)	a_R (fm)	W_0 (MeV)	R_I (fm)	a_I (fm)	χ^2/χ_0^2[b]
60.5	6.91	0.518	8.87	7.09	0.707	12.5
58.8	6.74	0.574	10.0	7.22	0.817	1.0
					0.967	1.8
		0.565				3.5
	7.16					5.0
67.6						6.8
			9.94			11.1
				7.15		11.8

[a] See footnote a in Table III for explanation of Table IV.
[b] $\chi_0^2 = 5.2$.

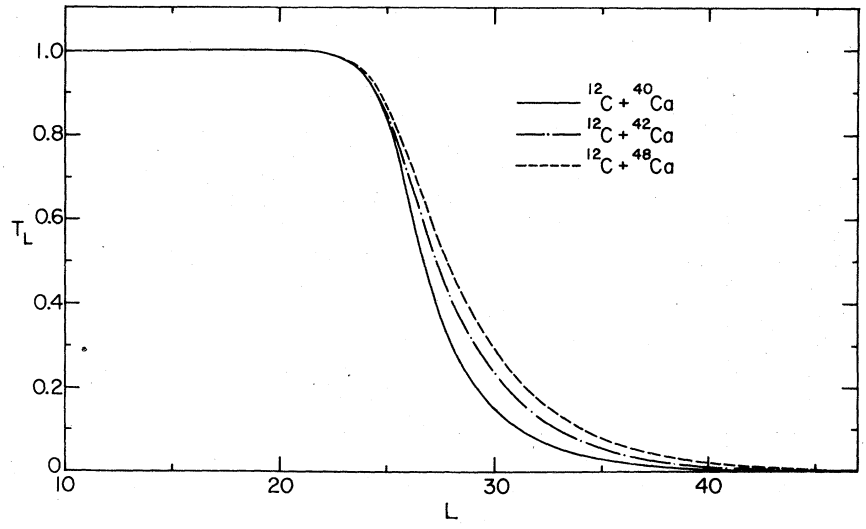

FIG. 3. Transmission coefficients, i.e., $T_L \equiv 1 - |S_L|^2$, for $^{12}C + ^{40,42,48}Ca$, respectively, calculated with the optical-model code PTOLEMY using parameters found in Table II.

TABLE V. Critical L values.

System	L_{cr} [a]	L_{cr} [b]	D [c] (fm)
^{12}C + ^{40}Ca	26.8	26.8	8.7
^{12}C + ^{42}Ca	27.3	27.1	8.8
^{12}C + ^{48}Ca	27.8	27.9	9.0

[a] $T_{L_{cr}} = \frac{1}{2}$ where $T_L = 1 - |S_L|^2 \equiv$ transmission coefficient for Lth partial wave.

[b] $L_{cr} = \eta \cot \theta_{cr}/2$ where $\eta = Z_1 Z_2 e^2/\hbar V$ and θ_{cr} is the critical angle where $\sigma/\sigma_R = \frac{1}{4}$.

[c] $D_{1/2} = (\eta/K)[1 + (L_{cr}/\eta + 1)^2]^{1/2} \equiv$ strong absorption radius.

B. Folded potential analysis

An attempt was made to see whether a folded potential derived from the density distributions of the ^{12}C and Ca nuclei could fit the data. In this model one calculates an ion-ion potential from a nucleon-nucleon interaction folded into the nuclear densities of the two ions. This model has been used with some success in fitting heavy-ion data[22] as well as light-ion data.[23] However, there are theoretical deficiencies in such an approach for heavy ions.[24] Core polarization, exchange effects, Pauli distortion, antisymmetrization, and density-dependent interaction effects are all absent from the folding prescription and yet may be important. In fact the present results indicate that for cross sections with as much structure as found in the ^{12}C + ^{40}Ca scattering, there is considerably more sensitivity to the shape of the real potential than is usual in other data fits. Problems with a double folding prescription in α and ^{3}He scattering have also been found,[25] though folding of a nucleon-α interaction with the target density gives good fits to α nucleus scattering and α-free nucleon scattering.[26] Unfortunately, no successful folding prescription exists for calculating the imaginary part of the optical potential which describes the absorption of elastic flux inside the nucleus. Generally the real and imaginary shapes are either taken to be identical or a Woods-Saxon geometry with three free parameters is used for the imaginary geometry.[27]

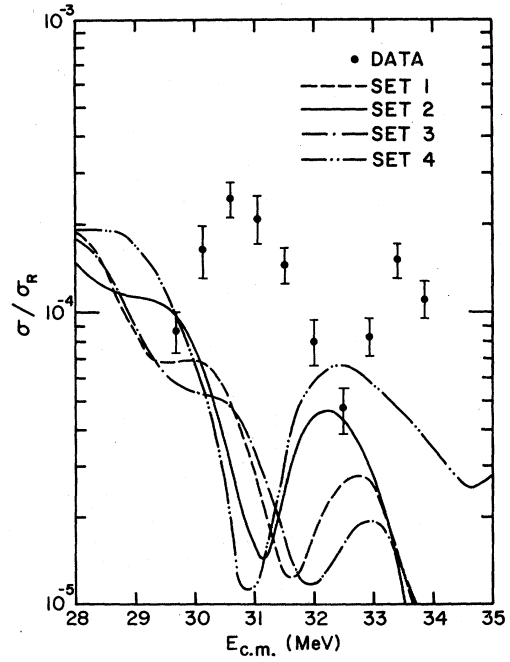

FIG. 4. ^{12}C + ^{40}Ca excitation function at 180° displayed with predictions of optical model using parameters taken from forward-angle fits to the data. See Table I.

The double-folded potential is given by

$$V(r) = \int d\vec{r}' \int d\vec{r}'' \rho(r'') V(|\vec{r} + \vec{r}'' - \vec{r}'|) \rho(r') \quad (1)$$

The method used for calculating the potential was that of Budzanowski.[23] The code PTOLEMY[17] was modified to use an arbitrarily shaped potential in optical-model calculations. Nuclear densities were constructed from single-particle wave functions generated in a Woods-Saxon well. Known binding energies, rms charge radii, and splittings of single-particle levels shown in Table VI were used to constrain the wave functions. The nucleon-nucleon interaction used initially was Satchler's which has a short-range repulsive core and a longer-range attractive part[21]:

$$V(r) = A \frac{e^{-r/r_1}}{r/r_1} + B \frac{e^{-r/r_2}}{r/r_2}, \quad (2)$$

where $r_1 = 0.25$ fm, $r_2 = 0.4$ fm, $A = 6315$ MeV, $B = -1961$ MeV.

A more general interaction would include a one-pion exchange potential (OPEP) part with a range of 1.41 fm. Considering only direct and not exchange terms of a nucleon-nucleon interaction, one finds that for $T = 0$, $S = 0$, $N = Z$ nuclei the OPEP terms do not contribute after averaging over spin and isopin. This leaves only the above two terms whose coefficients are determined from fits to G-matrix elements.[21] The long-range part of Eq. (2) simulates two-pion exchange while the short-range part has a range fixed to reflect hard-core repulsion in the nucleon-nucleon interaction.

Real potentials obtained with this interaction plus a Woods-Saxon imaginary well with three free parameters failed to reproduce the oscillations in the forward-angle data of ^{40}Ca as seen in Fig. 5. A single attractive Yukawa shape with an adjustable range was then tried as the n–n interaction. A one-pion-exchange range of 1.4 fm was tried first, but failed to produce any oscillatory structure in the angular distributions. A δ-func-

TABLE VI. Woods-Saxon bound-state wave function parameters.[a]

Nucleus		SE (MeV)[b]	$\sqrt{\langle R^2\rangle}$[c]	V_0 (MeV)[d]	V_{LSO} (MeV)[e]	R (fm)[f]
^{12}C	π	−15.957	2.45	68.4	9.2	2.60
	ν	−18.722		67.9	9.2	2.60
^{40}Ca	π	−8.3296	3.47	54.0	14.00	4.44
	ν	−15.6340		53.9	14.00	4.44
^{48}Ca	π	−15.807	3.47	58.9	12.35	4.66
	ν	−9.9510		45.0	12.35	4.66

[a] V_{LSO} and R were varied until the right charge radii and spin orbit splitting were obtained.
[b] Separation energies of last nucleon.
[c] RMS charge radii taken from electron scattering data.
[d] Depth of Woods-Saxon well used to calculate radial wave functions. Diffuseness of well was $a = 0.65$ fm.
[e] $V_{L\cdot S} = 4V_{LSO} \times [(\vec{L}\cdot\vec{S})/r] \times (d/dr)[1/(1+e^{(r-R)/a})]$.
[f] $R \equiv R_n = R_p = R_c$.

tion interaction or zero-range interaction also failed to fit the data. Other ranges were than tried until a reasonable fit was obtained as seen in Fig. 5; a value between 0.3 and 0.2 fm was required. Further calculations were performed with a range of 0.25 fm. The single Yukawa interaction as well as Satchler's are shown in Fig. 6.

Why such a modification in range is necessary is not understood. Since the important region in elastic scattering corresponds to a 5% overlap of the nuclear densities, the tails of the density distributions determine the important surface interaction region. The effects mentioned earlier, which are ignored in the calculations, possibly could account for the need of an *ad hoc* substitute for the modified nucleon-nucleon interaction. Renormalization of the depth of the folded potential does not remedy the poor fits with Satchler's interaction since in fitting the data the depth of the folded potential was allowed to vary. Typically, factors of 0.97 were required as shown in Table VII.

For ^{48}Ca the same folding prescription was used as for ^{40}Ca. The Yukawa interaction with a range of 0.25 fm was folded into the ^{12}C and ^{48}Ca densities to yield a real optical potential, and a three-

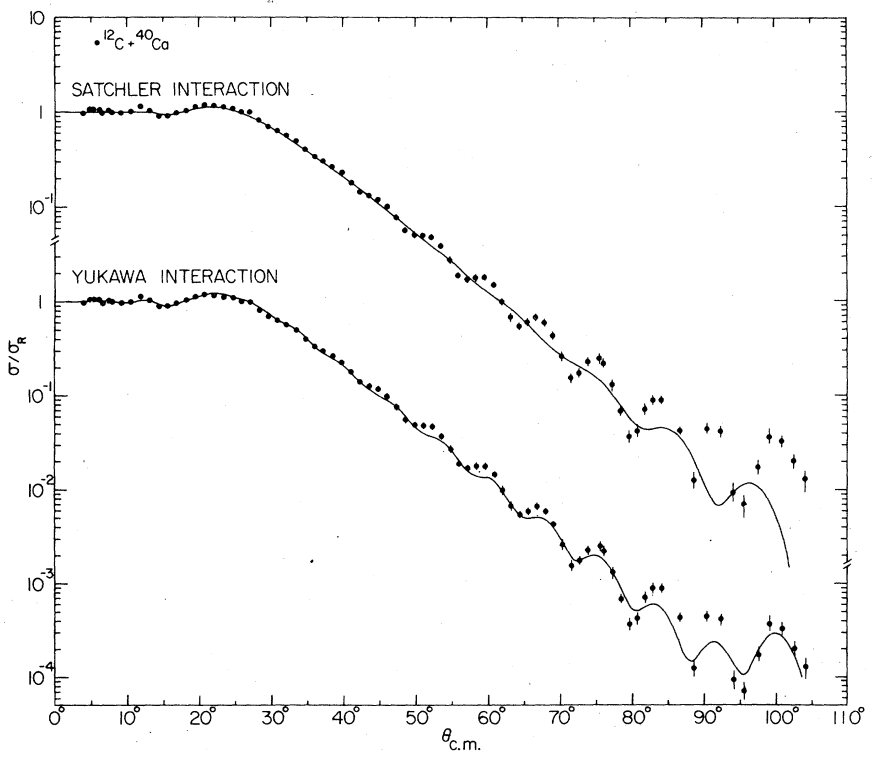

FIG. 5. (a) Folded-potential fit to ^{12}C + ^{40}Ca forward-angle data using a Woods-Saxon imaginary well. The normalization of the real well along with W_0, R_I, a_I were allowed to vary. The folded potential was generated from Satchler's nucleon-nucleon interaction. (b) Folded-potential fit to ^{12}C + ^{40}Ca data using a real potential generated with a Yukawa interaction of 0.25 fm range for the nucleon-nucleon interaction. See Fig. 6.

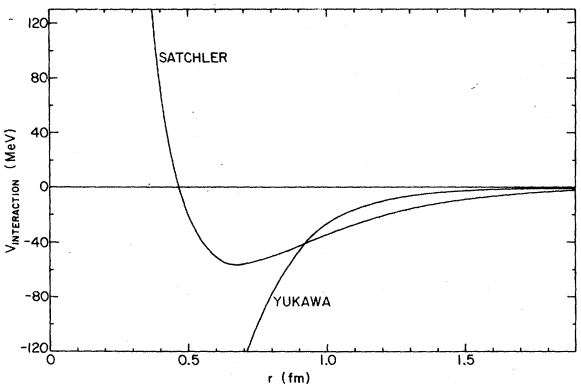

FIG. 6. Comparison of Yukawa and Satchler nucleon-nucleon interaction.

$$V_{\text{Satchler}}=\frac{Ae^{-r/r_1}}{r/r_1}+\frac{Be^{-r/r_2}}{r/r_2},$$

where $A=6315$ MeV, $B=-1961$ MeV, $r_1=0.25$ fm, and $r_2=0.4$ fm. $V_{\text{Yukawa}}=6380\ e^{-(r/r_y)}/r$, where $r_y=0.25$ fm.

parameter Woods-Saxon geometry was used for the imaginary well. The data here have a smooth, featureless behavior which was easily fitted, as shown in Fig. 7. Because the falloff in the data is smooth, the interaction of Satchler also fitted the data, but with a considerably stronger imaginary well.

The real well for ^{48}Ca generated by the Yukawa interaction with a 0.25-fm range is more diffuse than that for ^{40}Ca. Also, as was seen in the Woods-Saxon analysis (Fig. 8), the imaginary well for ^{48}Ca is very diffuse. The change in the real folded potential from ^{40}Ca probably arises from the extra nucleons in ^{48}Ca since in the folding prescription only the densities were changed. However, in fitting the data the imaginary potential is more important and no method for calculating it from the mass distribution is known. Nevertheless an attempt was made at calculating the effect of the $1f_{7/2}$ valence nucleons on the ^{12}C scattering from ^{48}Ca by adding to the real and imaginary potential of ^{12}C + ^{40}Ca a potential generated from the densities of the $1f_{7/2}$ nucleon and allowing these two strengths to vary independently. An attempt was also made to generate an imaginary potential from the densities by weighting the individual single-particle states according to their binding energies. One may expect that the nucleons in the loosely bound states are the easiest to excite and that they should contribute more heavily to the imaginary potential, while the most deeply bound ones would contribute little. This prescription did not work either though no adjustment of the ranges was tried. Consequently, how the extra nucleons change the shape of the imaginary well could not be determined. We can only surmise, as in the Woods-Saxon analysis, that the $1f_{7/2}$ nucleons play a crucial role similar to the one the extra nucleons play in the α plus ^{40}Ca and ^{44}Ca angular distributions.

C. Localization of the interaction region

The assumption that only the surface region of the real potential is important was tested by using an exponential cutoff[22] of 0.2 fm diffuseness with the potentials of Table II. The inner cutoff consisted of multiplying the real well by $\exp[(R-R_{CI})/\lambda]$ inside the cutoff radius R_{CI} and leaving the well unchanged outside R_{CI}. The outer cutoff consisted of multiplying the real potential by $\exp[-(R-R_{CO})/\lambda]$ outside the cutoff radius R_{CO} and leaving the well unchanged inside R_{CO}. The χ^2 with the real well cutoff was divided by that for the complete Woods-Saxon potential. A strong deterioration in χ^2 for ^{40}Ca was seen between 2 and 10 fm as is shown in Fig. 9. The sensitive region for ^{42}Ca is the same as for ^{40}Ca, while for ^{48}Ca the fits were sensitive only to the region between 3 and 10 fm. Similar results were obtained with the ^{40}Ca potential sets 3($V_0=60.5$ MeV) and 4($V_0=502$ MeV).

D. Other work

Differences in the behavior of the elastic angular distributions for ^{12}C on ^{40}Ca versus ^{12}C on ^{44}Ca were observed by Morgan and Fletcher at Florida State University.[18] These differences can also be parametrized by a more diffuse imaginary potential.

TABLE VII. Folded potential fit parameters.

System	Interaction	Real depth in MeV	Renormalization factor	W_0 (MeV)	R_I (fm)	a_I (fm)	χ^2/χ_0^2 [a]
^{12}C + ^{40}Ca	Satchler	570.7	0.97	12.1	7.36	0.689	3.3
^{12}C + ^{40}Ca	Yukawa [b]	6379.9	...	16.7	7.04	0.497	1.6
^{12}C + ^{48}Ca	Satchler	574.1	0.97	16.4	7.35	0.638	1.1
^{12}C + ^{48}Ca	Yukawa [b]	3074.8	...	45.6	5.84	0.844	1.0

[a] $\chi_0^2(^{40}\text{Ca})=1.6$, value of best Woods-Saxon fit. $\chi_0^2(^{48}\text{Ca})=5.2$, value of best Woods-Saxon fit.
[b] Yukawa range = 0.25 fm.

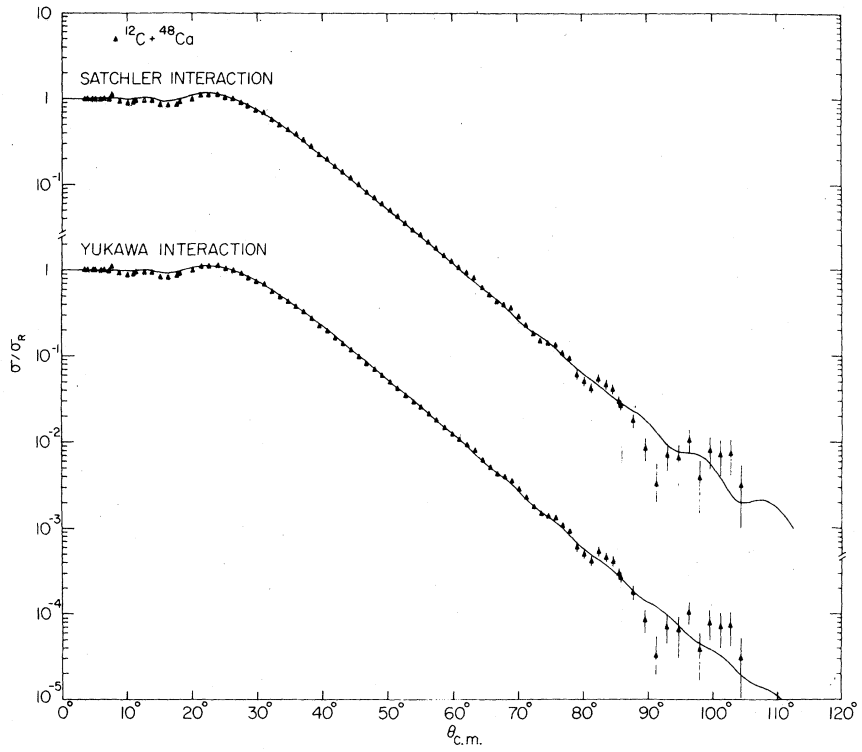

FIG. 7. (a) Fit to $^{12}C + ^{48}Ca$ data using folded potential generated from Yukawa interaction of 0.25 fm range. The real depth was allowed to vary as well as W_0, R_I, and a_I. (b) Fit to $^{12}C + ^{48}Ca$ data using Satchler's interaction in a folding prescription with four free parameters: one for the real well depth and W_0, R_I, a_I.

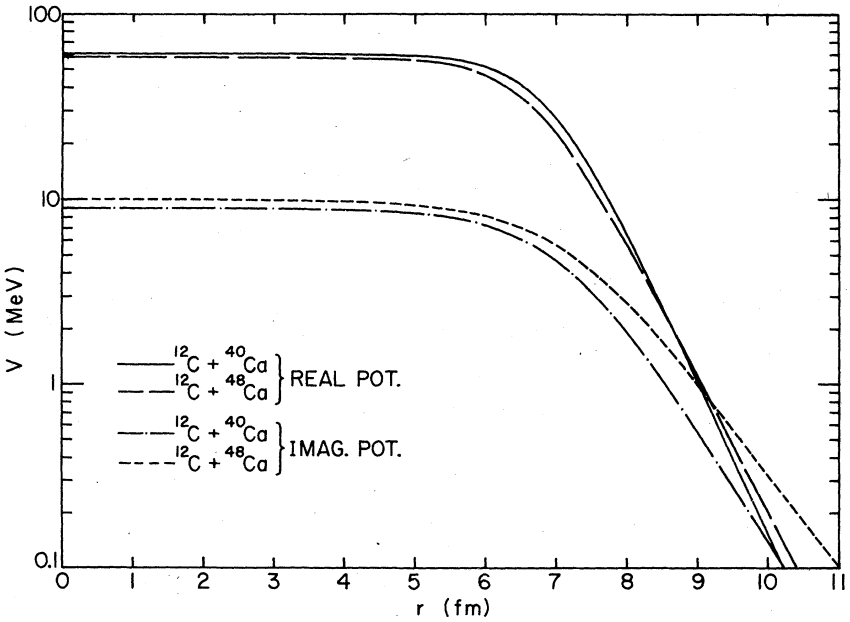

FIG. 8. Woods-Saxon real and imaginary potentials used in fitting $^{12}C + ^{40}Ca$ and $^{12}C + ^{48}Ca$ data shown in Fig. 1.

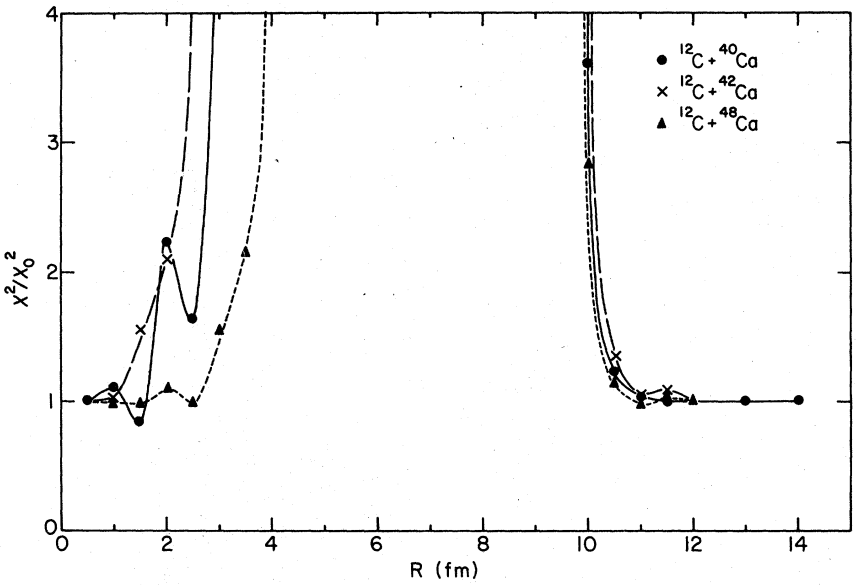

FIG. 9. Sensitive region of Woods-Saxon wells to exponential cutoffs for ^{40}Ca, ^{42}Ca, ^{48}Ca. Range of cutoff was $\lambda = 0.2$ fm.

IV. CONCLUSIONS

There is a clear difference observed between the scattering of ^{12}C from ^{40}Ca and from $^{42,48}Ca$. The oscillatory structure in the angular distribution becomes much weaker and disappears as valence nucleons are added in the $1f_{7/2}$ shell.

Optical-model analyses indicate that these differences can be attributed to the increasing diffuseness of the absorptive imaginary well as more reaction channels open up involving the surface-peaked valence nucleons. The structure in the ^{40}Ca angular distribution makes this data set a much more sensitive probe of *a priori* real potential parameters (folding potentials) derived from mass distributions. It is found that the previously used range for an attractive Yukawa shape (0.4 fm) cannot fit the data; a range of 0.25 fm does fit adequately. Simple folding prescriptions do not appear to work for the imaginary potential.

The sharper and smaller imaginary well in ^{40}Ca allows surface partial waves to resonate inside the real well. The structure in the back-angle excitation function[16] could be evidence for such shape resonances. A simple condition of an integral number of wavelengths fitting inside the real well seems to describe the spacings of the resonances. If shape resonances are responsible for the structure in the back-angle excitation function then their effects might be felt in other reaction channels. The potentials for ^{48}Ca which fit the structureless exponential falloff of the forward-angle data predict a much lower back-angle cross section than the ones for ^{40}Ca, and no resonant structure.

ACKNOWLEDGMENTS

I wish to acknowledge and thank John Schiffer for the support and guidance given me during this work. I also wish to thank the tandem technicians for their help. This work was performed under the auspices of the Department of Energy. This work is submitted in partial fulfillment of the requirements for the degree of Doctor of Philosophy from the University of Chicago.

[1]N. S. Wall, Phys. Rev. C 14, 2326 (1976).
[2]D. Agassi and N. S. Wall, Phys. Rev. C 7, 1368 (1973).
[3]R. H. Siemssen, in Proceedings of the International Conference on Resonances in Heavy Ion Reactions, Hvar, Yugoslavia (unpublished).
[4]K. W. McVoy, Phys. Rev. C 3, 1104 (1971).
[5]K. A. Eberhard, Phys. Lett. 33B, 343 (1970).
[6]F. Michel and R. Vanderpoorten, Phys. Rev. C 16, 142 (1977).
[7]G. Gaul, H. Ludecke, R. Santo, H. Schmeing, and R. Stock, Nucl. Phys. A137, 177 (1969).
[8]P. Sperr, S. Vigdor, Y. Eisen, W. Henning, D. G. Kovar, T. R. Ophel, and B. Zeidman, Phys. Rev. Lett. 36, 405 (1976).
[9]P. Sperr, T. H. Braid, Y. Eisen, D. G. Kovar, F. W. Prosser, Jr., J. P. Schiffer, S. L. Tabor, and S. Vigdor, Phys. Rev. Lett. 37, 321 (1976).
[10]E. Colombo, R. Deleo, J. L. Escudie, E. Fabrici, S.

Michelettim, M. Pignanelli, and F. Resuini, report (unpublished).
[11]K. A. Eberhard, M. Wit, J. Schiele, W. Trombik, W. Zipper, and J. P. Schiffer, Phys. Rev. C 14, 2332 (1976).
[12]P. Braun-Munzinger, G. M. Berkowitz, T. M. Cormier, C. M. Jachcinski, J. W. Harris, J. Barette, and M. J. LeVine, in *Proceedings of the Symposium on Heavy Ion Elastic Scattering*, University of Rochester, edited by R. M. DeVries (Univ. of Rochester, Ithaca, 1977), p. 85.
[13]R. DeVries, in *Proceedings of the Symposium on Heavy Ion Elastic Scattering*, University of Rochester, edited by R. M. DeVries (Univ. of Rochester, Ithaca, 1977), p. 1; M. R. Clover, R. M. DeVries, R. Ost, N. J. A. Rust, R. N. Cherry, Jr., and H. E. Gove, Phys. Rev. Lett. 40, 1008 (1978).
[14]J. S. Blair, Phys. Rev. 95, 1218 (1954).
[15]W. E. Frahn, Ann. Phys. (N.Y.) 78, 524 (1972); Phys. Rev. Lett. 26, 568 (1971).
[16]K. Ford and J. A. Wheeler, Ann. Phys. (N.Y.) 7, 259 (1959).
[17]M. H. Macfarlane and Steven C. Piper, PTOLEMY, Report No. ANL-76-11 Rev. 1 (unpublished).
[18]G. R. Morgan and N. R. Fletcher, report (unpublished).
[19]W. Henning, Y. Eisen, J. R. Erskine, D. G. Kovar, and B. Zeidman, Phys. Rev. C 15, 292 (1977).
[20]T. R. Renner, J. P. Schiffer, D. Horn, G. C. Ball, and W. G. Davies, Phys. Rev. C 18, 1927 (1978).
[21]G. R. Satchler and W. G. Love, Phys. Lett. 65B, 415 (1976).
[22]G. R. Satchler, in Proceedings of the Symposium on Macroscopic Features of Heavy-Ion Collisions, Argonne National Laboratory Report ANL-PHY-76-2, 1976 (unpublished), p. 33.
[23]A. Budzanowski, A. Budek, K. Grotowski, and A. Strzalkowski, Phys. Lett. 32B, 431 (1970).
[24]J. Fleckner and U. Mosel, Nucl. Phys. A277, 170 (1977); P. G. Zint and U. Mosel, Phys. Rev. C 14, 1488 (1976).
[25]C. J. Batty, E. Friedman, and D. F. Jackson, Nucl. Phys. A175, 1 (1971).
[26]P. Mailandt, J. S. Lilley, and G. W. Greenlees, Phys. Rev. C 8, 2189 (1973).
[27]W. G. Love, in *Proceedings of the Symposium on Heavy Ion Elastic Scattering*, University of Rochester, edited by R. M. DeVries (Univ. of Rochester, Ithaca, 1977), p. 266.